Electronic Supplementary Material (ESI) for Journal of Materials Chemistry C.

Supporting Information

Synthesis of continuous MoS_2:Er films and their enhanced NIR photoresponse for photo communication

Lei Wang,[a, b] Xiaohong Ji,[a] and Qinyuan Zhang[a,b*]*

[a.]School of Materials Science and Engineering, South China University of Technology, 510641, China.
[b.]State Key Laboratory of Luminescent Material and Devices, South China University of Technology, 510641, China.
**E-mail: jxhong@scut.edu.cn; qyzhang@scut.edu.cn.*

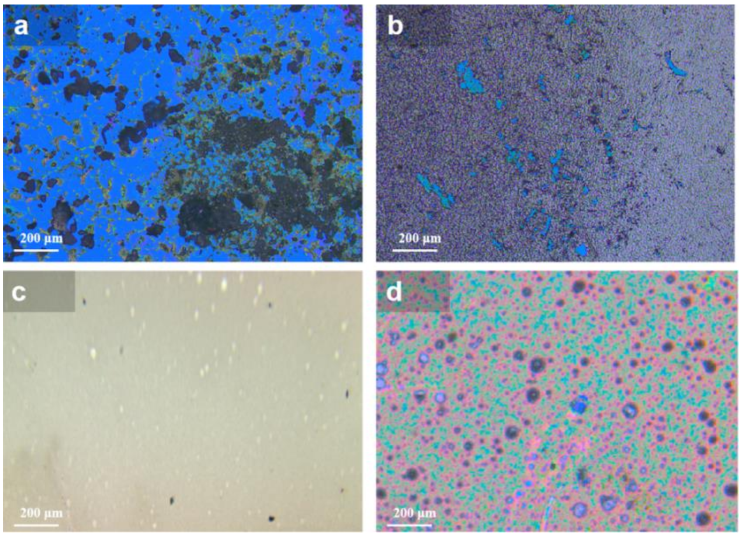

Figure S1 Influence of the amount of $C_6H_8O_7$ on the morphology of the film. Optical images of MoS_2:Er films with adding a) 300 mg, b) 500 mg, c) 700 mg, and d) 900 mg $C_6H_8O_7$ into the precursor solutions, respectively. Too little dosage would lead to the insufficient viscosity of the precursor solution and the incomplete dissolution of the precipitate Er_2MoO_6, while too much dosage would lead to more holes in the film due to the large amount of gas produced by the decomposition of $C_6H_8O_7$.

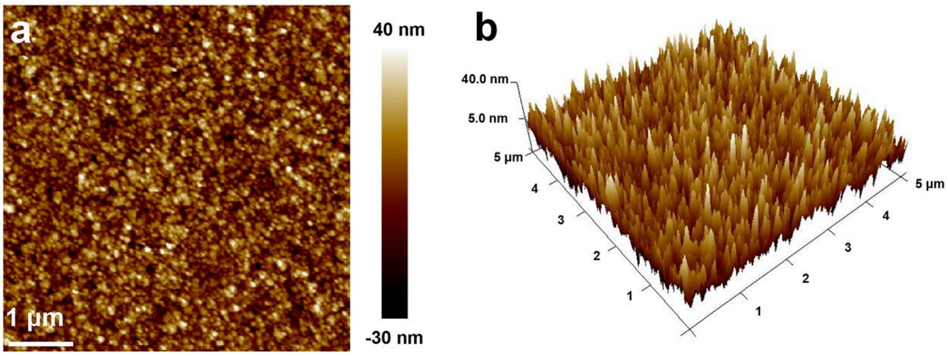

Figure S2 (a) 2D and (b) 3D AFM image of the MoS_2:2mol%Er film.

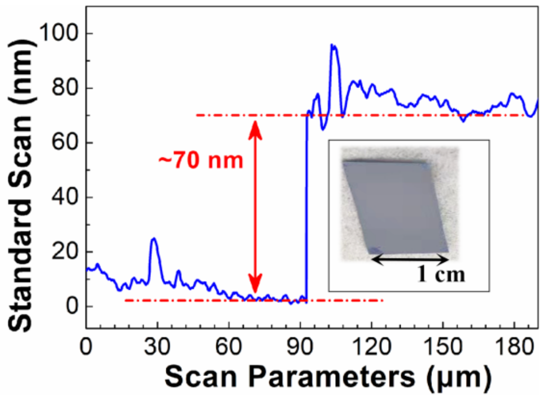

Figure S3 Height curve of the MoS_2:2mol%Er film.

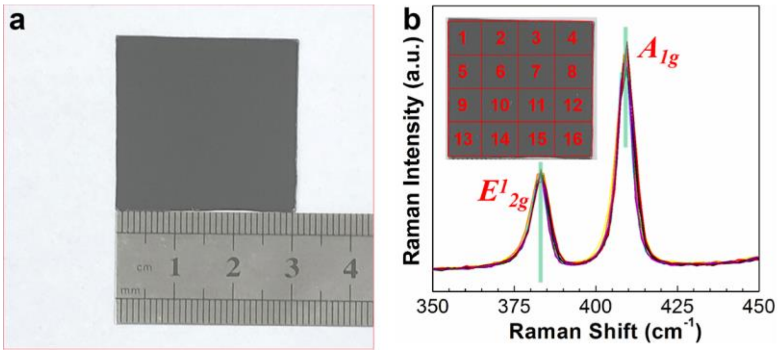

Figure S4 (a) Digital photo of the MoS_2:2mol%Er film on a 3×3 cm^2 300-nm-SiO_2/Si substrate. (b) Raman spectra of different regions on the substrate. The inset in (b) presents the different regions on the substrate. The Raman spectra exhibit generally consistent peak positions and intensities.

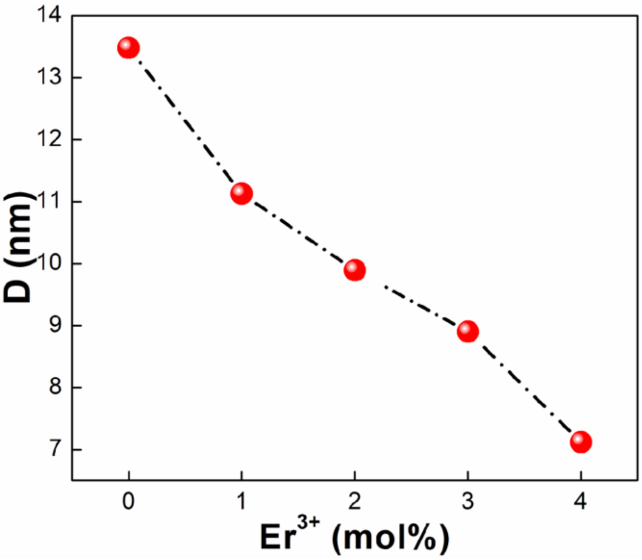

Figure S5 Average grain size dependence of Er^{3+} doping concentration. The average grain size (D) was obtained from the XRD patterns in terms of diffraction of (002) planes and the Scherrer Formula: $D=K\lambda/(\beta\cos\gamma)$, where K is the Scherrer constant, λ is the X-ray wavelength, β is the line broadening at FWHM in radians, and γ is the Bragg's angle in degrees.[2] The decrease in particle size would lead to an enhanced lattice scattering for the carrier.[3]

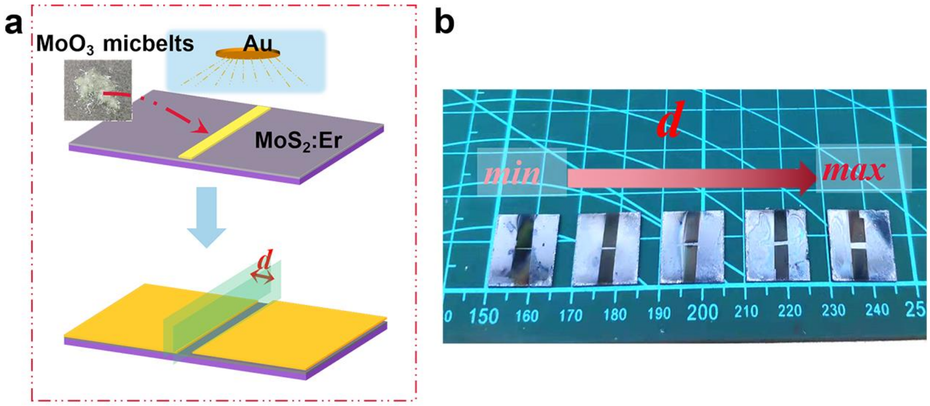

Figure S6 a) Schematic diagram showing the synthesis process of devices with different electrode distances. The self-synthesized MoO_3 microbelt was used as the mask, so the electrode distance of the photodetector device can be flexibly controlled. b) The camera photos of obtained devices with different electrode distances.

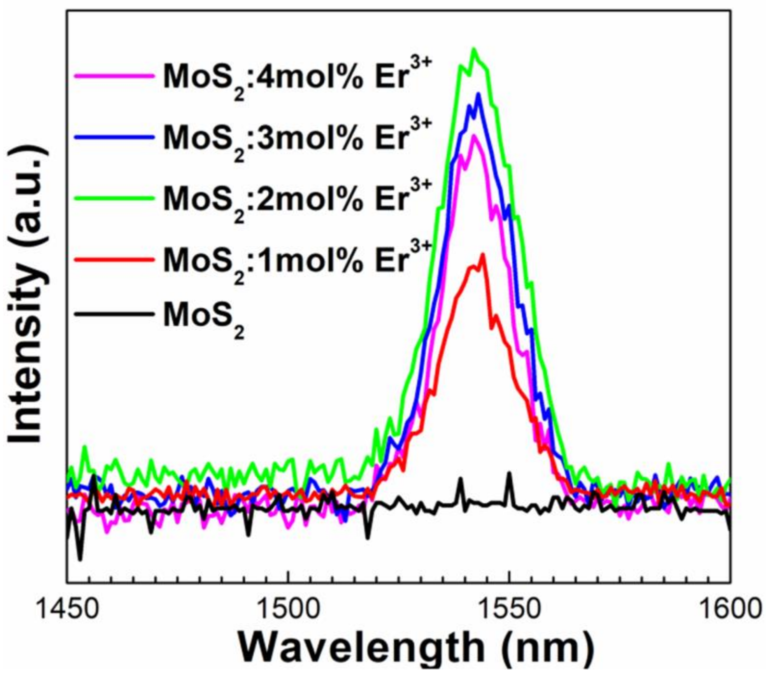

Figure S7 The emission intensity variation in $^4I_{13/2}\rightarrow{}^4I_{15/2}$ energy transition of Er^{3+} ions at different doping concentrations. The photoluminescence spectra were excited by a 980 nm laser.

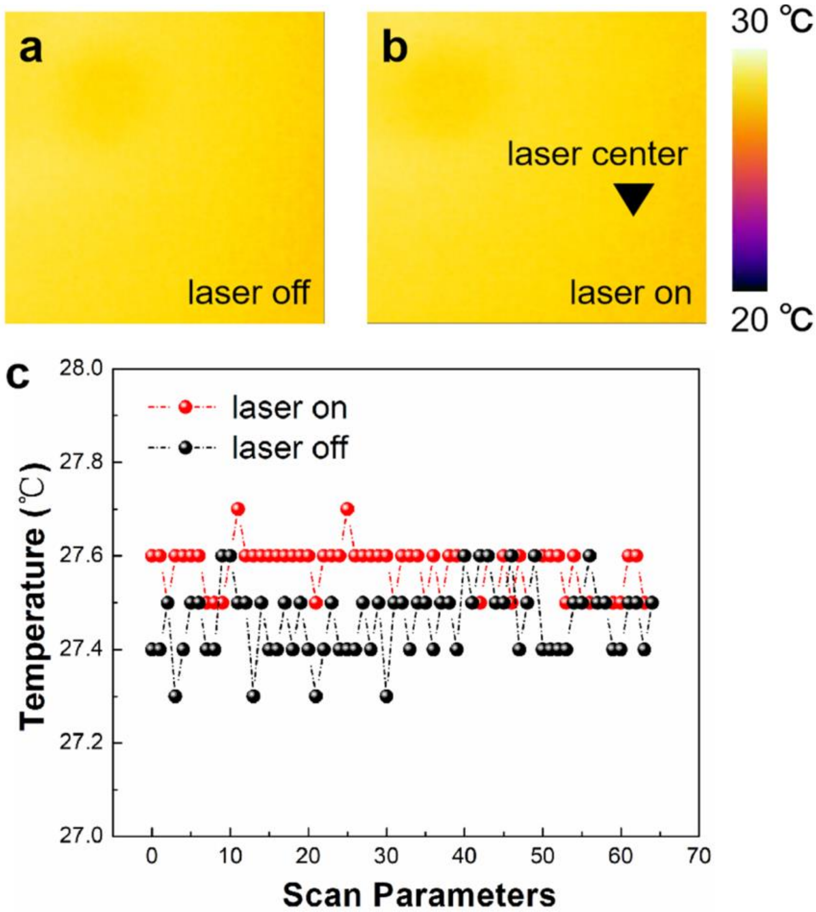

Figure S8 2D infrared images of MoS_2:2mol%Er film in the a) "off" and b) "on" states (980 nm@20 mW/cm^2). c) Temperature distribution curves of MoS_2:2mol%Er film in the "off" and "on" states.

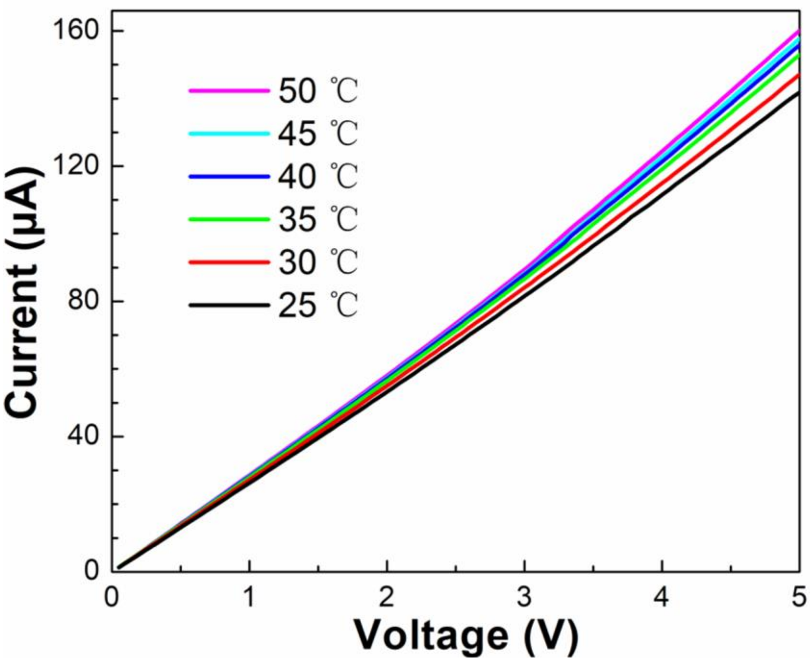

Figure S9 Temperature-dependent *I-V* curves of the device. The temperature has a slight effect on the resistance. Thus, the enhanced photoelectric performance is not related to the NIR thermal effect.

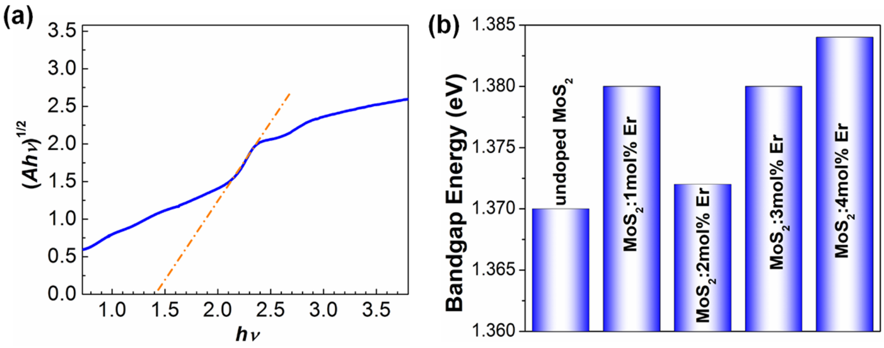

Figure S10 (a) Replot of absorption spectra of MoS_2:Er films. (b) Change in the bandgap as a function of doping concentration.

The bandgap energy (E_g) can be deduced from the absorption spectra according to the formula

$$[F(R'_\infty)*h\nu]^{1/2} = B(h\nu - E_g)$$

where R'_∞ is the absolute reflectance of the sample at an infinite thickness, h is Planck's constant, ν is the photon frequency, and B is the proportionality constant.[4] The bandgap energy value of the MoS_2:Er films is ~1.38 eV. The negligible difference in E_g for various concentrations of Er-doped MoS_2 films demonstrates the weak effect of Er^{3+} doping on the bandgap width of the host.

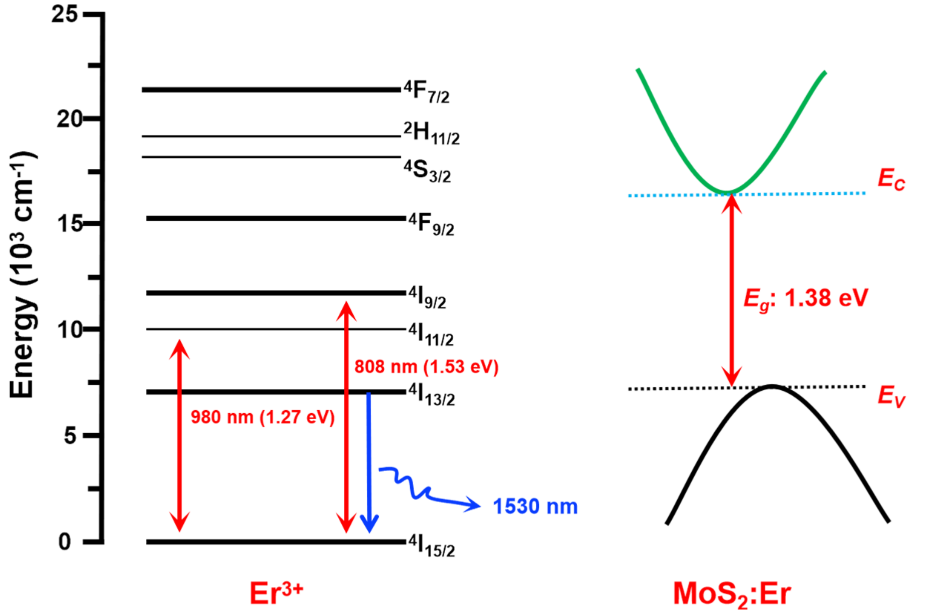

Figure S11 Energy levels of Er^{3+} ions and band structure of the bulk MoS_2:Er.[5]

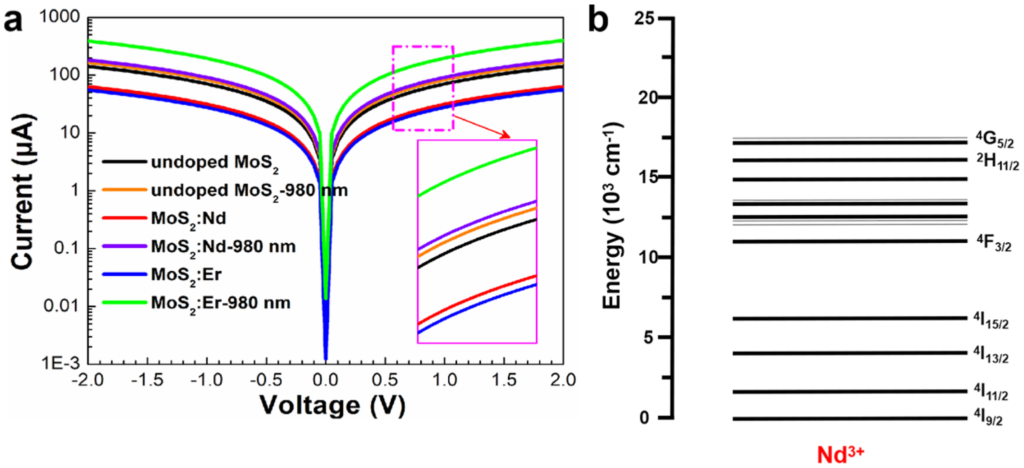

Figure S12 a) *I-V* curves of the undoped MoS_2, MoS_2:2mol%Nd and MoS_2:2mol%Er. b) Energy levels of Nd^{3+} ions.[6] The gain of the photoconductance can be obtained by doping Nd^{3+} ions (R_{dark}/R_{light} ratio: 2.91), which is lower than doping Er^{3+} ions.

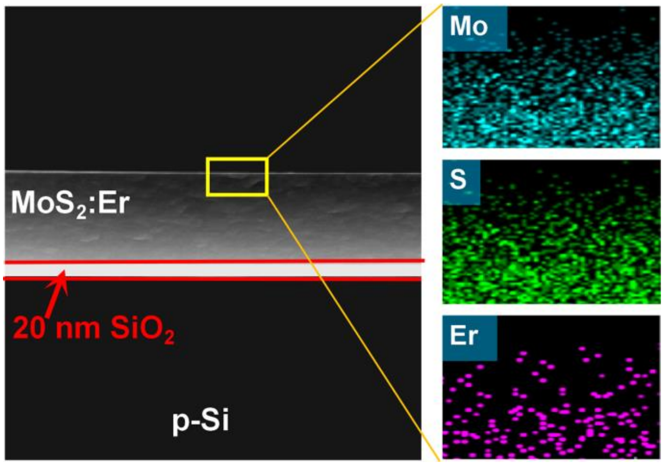

Figure S13 Cross-section SEM image of the MoS_2:Er/SiO_2/p-Si heterojunction and EDS elemental mapping images of Mo, S, and Er. The selected area was marked by a yellow box in the SEM image.

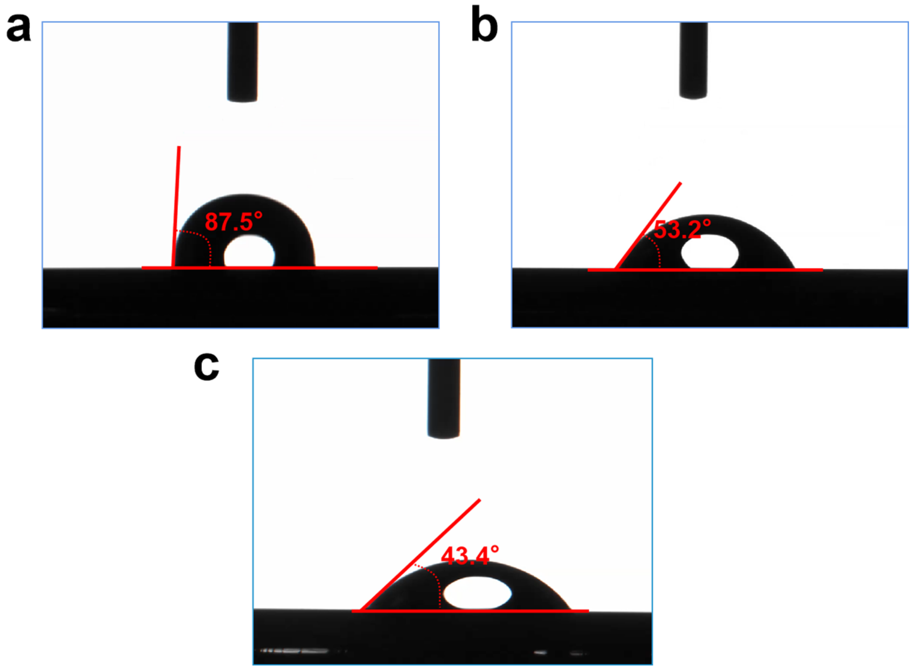

Figure S14 Hydrophilic test results of a) untreated Si substrate, b) Si substrate treated by NaOH ethanol solution, and c) 20-nm-SiO_2/Si substrate. Water contact angles were measured to be 87.5°, 53.2°, and 43.4°, respectively.

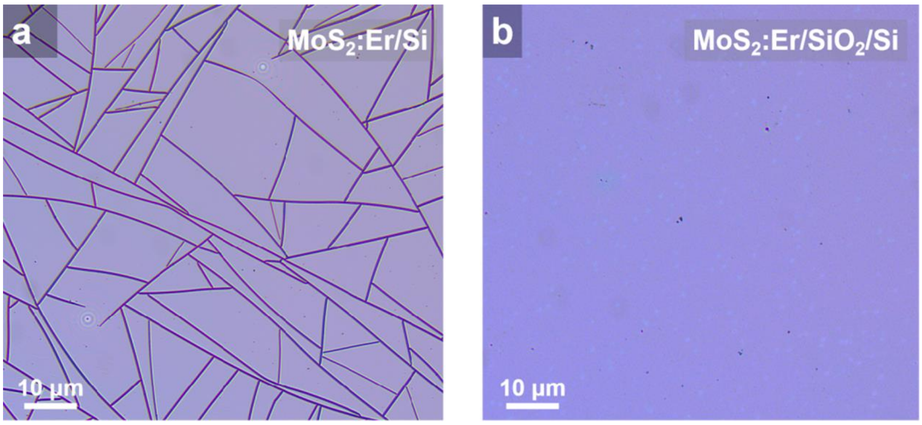

Figure S15 Optical images of MoS_2:Er films on the a) treated Si substrate and b) 20-nm-SiO_2/Si substrate.

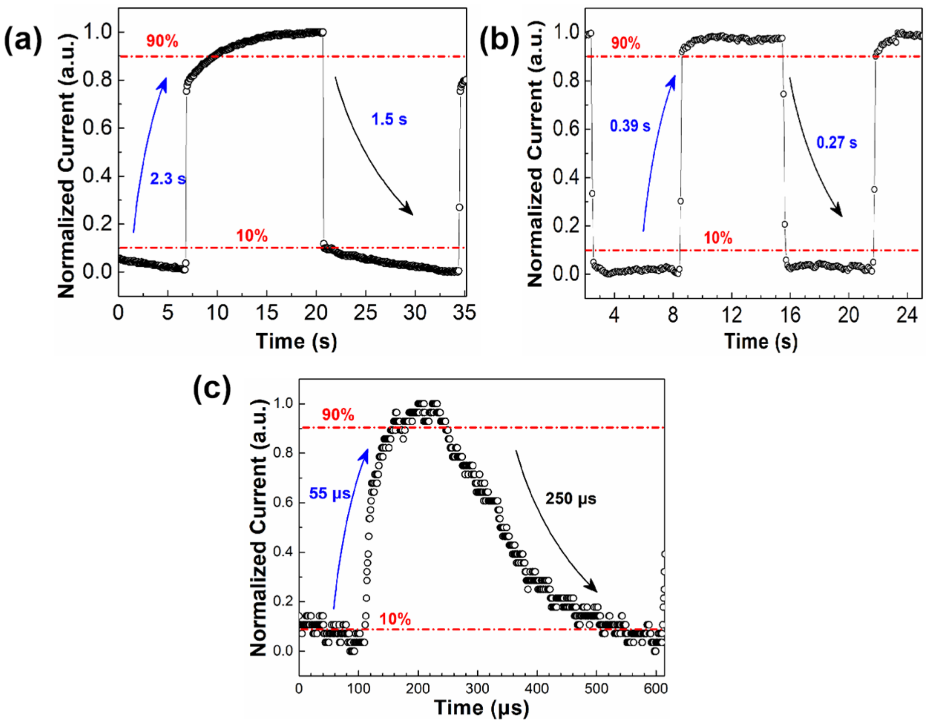

Figure S16 Typical rise and fall processes of MoS_2:Er-based device a) without SiO_2 layer, b) with 5-nm SiO_2 layer and c) with 30-nm SiO_2 layer.

Table S1 The key performance parameters of the MoS_2-based NIR photodetectors. Here, λ (nm), R (mA W^{-1}), D^* (Jones) and t_r/t_f, are the light wavelength, the responsivity, the detectivity, and the rise/fall time, respectively.

Structure	Voltage (V)	λ (nm)	R^*	D^*	t_r/t_f	Ref.
MoS_2/p-Si	-2	808	746	6×10^{11}	178µs/198µs	7
MoS_2/PbS	1	850	5.4×10^{7}	10^{11}	950µs/1ms	8
MoS_2/p-Si	6	850	10	4.53×10^{10}	78µs/76µs	9
Au@MoS_2/p-Si	4	800	3×10^{4}	-	20ms/20ms	10
MoS_2/p-Si	-9	850	1.78×10^{7}	10^{13}	1.44ms/1.45ms	11
MoS_2/PbS@Au	4.5	1064	1.22×10^{3}	1.56×10^{9}	>1s/>1s	12
MoS_2/α-$MoTe_2$	-	800	38	-	25ms/-	13
2D Te/MoS_2	8	980	2.84×10^{4}	2.7×10^{10}	-	14
PbSe/MoS_2	3	808	$1..97\times10^{4}$	2.65×10^{10}	0.38s/0.86s	15
MoS_2/p-Si	-4	850	-	-	2ms/5ms	16
MoS_2/Al_2O_3/p-GaAs	-0.1	1064	143.2	3.32×10^{10}	12µs/32µs	17
MoS_2@$CsPbBr_3$ QDs/Si	-3	808	975	6.56×10^{11}	6.8ms/6.7ms	18
MoS_2/SnS	1	808	2.44	5.94×10^{7}	0.69s/0.65s	19
MoS_2/$NaYF_4$	-15	980	0.1	10^{8}	8ms/14ms	20
($NaYF_4$:Yb/Er@Na YF_4:Nd/Yb)/MoS_2	1	980	10.5		7.9s/2.9s	21
MoS_2:Er/SiO_2/p-Si	**-0.5**	**980**	**46.7**	**3.67×10^{10}**	**1.4µs/152µs**	**This work**

References

1 M. Kim, J. Seo, J. Kim, J. S. Moon, J. Lee, J. Kim, J. Kang, H. Park, *ACS Nano*, 2021, **15**, 3038-3046.

2 U. Holzwarth and N. Gibson, *Nat. Nanotechnol.*, 2011, **6**, 534.

3 J. Kim, Y. Song, T. Kim, K. Cho, J. Pak, B. Y. Choi, J. Shin, S. Chung and T. Lee, *Nanotechnology*, 2017, **28**, 41L-47L.

4 M. Desseigne, N. Dirany, V. Chevallier and M. Arab, *Appl. Surf. Sci.*, 2019, **483**, 313-323.

5 M. Lun, W. Wu, Z. Xing, H. Song, Y. Wang, W. Li, B. Chu and Q. He, *J. Lumin.*, 2020, **223**, 117189.

6 A. J. Jebathew, M. Karunakaran, K. D. A. Kumar, S. Valanarasu, V. Ganesh, M. Shkir, S. Alfaify and A. Kathalingam, *Physica B: Condensed Matter*, 2019, **572**, 109-116.

7 J. Guo, S. Li, Y. Ke, Z. Lei, Y. Liu, L. Mao, T. Gong, T. Cheng, W. Huang and X. Zhang, *Scripta Mater.*, 2020, **176**, 1-6.

8 S. Pak, Y. Cho, J. Hong, J. Lee, S. Lee, B. Hou, G. An, Y. Lee, J. E. Jang, H. Im, S. M. Morris, J. I. Sohn, S. Cha and J. M. Kim, *ACS Appl. Mater. Inter.*, 2018, **10**, 38264-38271.

9 J. Choi, H. Y. Jang, A. R. Kim, J. Kwon, B. Cho, M. H. Park and Y. Kim, *Nanoscale*, 2021, **13**, 672.

10 Y. Li, J. G. Distefano, A. A. Murthy, J. D. Cain, E. D. Hanson, Q. Li, F. C. Castro, X. Chen and V. P. Dravid, *ACS Nano*, 2017, **11**, 10321-10329.

11 J. Deng, Z. Guo, Y. Zhang, X. Cao, S. Zhang, Y. Sheng, H. Xu, W. Bao and J. Wan, *IEEE Electr. Device L.*, 2019, **40**, 423-426.

12 S. Qin, H. Xu, M. Liu, N. Ali, Y. Chen, S. Zhao and H. Wu, *Appl. Surf. Sci.*, 2022, **585**, 152594.

13 A. Pezeshki, S. H. H. Shokouh, T. Nazari, K. Oh and S. Im, *Adv. Mater.*, 2016, **28**, 3216-3222.

14 J. Yao, F. Chen, J. Li, J. Du, D. Wu, Y. Tian, C. Zhang, J. Yang, X. Li and P. Lin, *J. Mater. Chem. C*, 2021, **9**, 13123-13131.

15 M. Peng, Y. Tao, X. Hong, Y. Liu, Z. Wen and X. Sun, *J. Mater. Chem. C*, 2022, **10**, 2236-2244.

16 H. Y. Jang, J. H. Nam, J. Yoon, Y. Kim, W. Park and B. Cho, *Nanotechnology*, 2020, **31**, 225205.

17 J. Qu and J. Chen, *Micro and Nanostructures*, 2022, **166**, 207231.

18 L. Guo, Y. Gu, Z. Yang, S. Tian, X. San, J. Liu, L. Gao, S. Qiao and S. Wang, *Adv. Mater. Interfaces*, 2021, **8**, 2002231.

19 H. Yu, Y. Xie, J. Wei, P. Zhang and Z. Cui, *Adv. Mater. Interfaces*, 2022, **9**, 2200896.

20 Y. Zhang, J. Wang, B. Wang, J. Shao, J. Deng, C. Cong, L. Hu, P. Tian, R. Liu, S. Zhang, and Z. Qiu, *Adv. Optical Mater.*, 2018, **6**, 1800660.

21 N. Zhou, B. Xu, L. Gan, J. Zhang, J. Han and T. Zhai, *J. Mater. Chem. C*, 2017, **5**, 1591-1595.